PCCP

Cite this: *Phys. Chem. Chem. Phys.*, 2011, **13**, 16973–16986

www.rsc.org/pccp

PERSPECTIVE

Computational and spectroscopic studies of organic mixed-valence compounds: where is the charge?†

Martin Kaupp,*[a] Manuel Renz,[a] Matthias Parthey,[a] Matthias Stolte,[bc] Frank Würthner[bc] and Christoph Lambert*[bc]

Received 1st June 2011, Accepted 3rd August 2011
DOI: 10.1039/c1cp21772k

This article discusses recent progress by a combination of spectroscopy and quantum-chemical calculations in classifying and characterizing organic mixed-valence systems in terms of their localized *vs.* delocalized character. A recently developed quantum-chemical protocol based on non-standard hybrid functionals and continuum solvent models is evaluated for an extended set of mixed-valence bis-triarylamine radical cations, augmented by unsymmetrical neutral triarylamine-perchlorotriphenylmethyl radicals. It turns out that the protocol is able to provide a successful assignment to class II or class III Robin-Day behavior and gives quite accurate ground- and excited-state properties for the radical cations. The limits of the protocol are probed by the anthracene-bridged system **8**, where it is suspected that specific solute–solvent interactions are important and not covered by the continuum solvent model. Intervalence charge-transfer excitation energies for the neutral unsymmetrical radicals are systematically overestimated, but dipole moments and a number of other properties are obtained accurately by the protocol.

1. Introduction

Localized or delocalized is the crucial question in mixed valence (MV) systems. In this article we will address this question by DFT computational methods. Mixed valency is a topic typically associated with binuclear transition metal complexes, their most prominent example being the Creutz–Taube ion. However, there are an increasing number of purely organic systems that may be conceived as mixed valence systems. These MV compounds are widely used as simple model systems in order to investigate basic aspects of electron transfer (ET).[1–4] MV systems usually consist of two or more redox centers with different oxidation states that are connected by conjugated or non-conjugated bridges (see Scheme 1). Typical redox centers are *e.g.* triarylamines,[5–10] perchlorotriphenylmethyl radicals,[11–13] hydrazines,[14,15] dimethoxybenzenes,[16,17] or quinones.[18,19] ET may proceed between the redox centers *via* the bridge, thermally or optically induced. The optical ET is associated with the so-called intervalence charge transfer (IV-CT) band which usually appears in the NIR. Among the various issues that have been investigated are the distance dependence of ET, the influence of local bridge states (electron rich *vs.* electron-deficient),[7,8] temperature,[20,21] solvent[22,23] and counter ion influences[24] *etc.*

A major aspect in MV systems concerns the shape of the ground and excited state potentials. In the simplest case of a MV system with two redox centers this may be either a double well potential (so called Robin-Day Class II) or a single well potential (Class III). The discrimination between these two classes is crucial as in Class II compounds the charge is localized on one redox center, and charge transfer to the other redox center is possible, while in Class III the charge is delocalized over both redox centers (and possibly the bridge). A simple two-state model may serve to illustrate the situation: in the special degenerate case, the adiabatic potential energy surfaces (PES) of the ground state (a) and the excited state (b) of a MV system with two redox centers (=two redox states) can be calculated by solving secular eqn (1) where harmonic

Scheme 1 MV system with two redox centers (circles) and the connecting bridge (bar). The different colors illustrate the different redox states of the redox centers, the different sizes illustrate the geometrical differences of charged *vs.* neutral redox centers.

[a] *Technische Universität Berlin, Institut für Chemie, Theoretische Chemie, Sekr, C7, Straße des 17, Juni 135, 10623 Berlin, Germany. E-mail: martin.kaupp@tu-berlin.de*
[b] *Institut für Organische Chemie, Universität Würzburg, Am Hubland, 97074 Würzburg, Germany. E-mail: lambert@chemie.uni-wuerzburg.de*
[c] *Wilhelm-Conrad-Röntgen Research Center for Complex Material Systems, 97074 Würzburg, Germany*

† Electronic supplementary information (ESI) available: Computed ground and excited state properties for **1–17** (Tables S1–S17) as well as Cartesian coordinates of all optimized structures (**5–17**, Table S19) are provided. See DOI: 10.1039/c1cp21772k

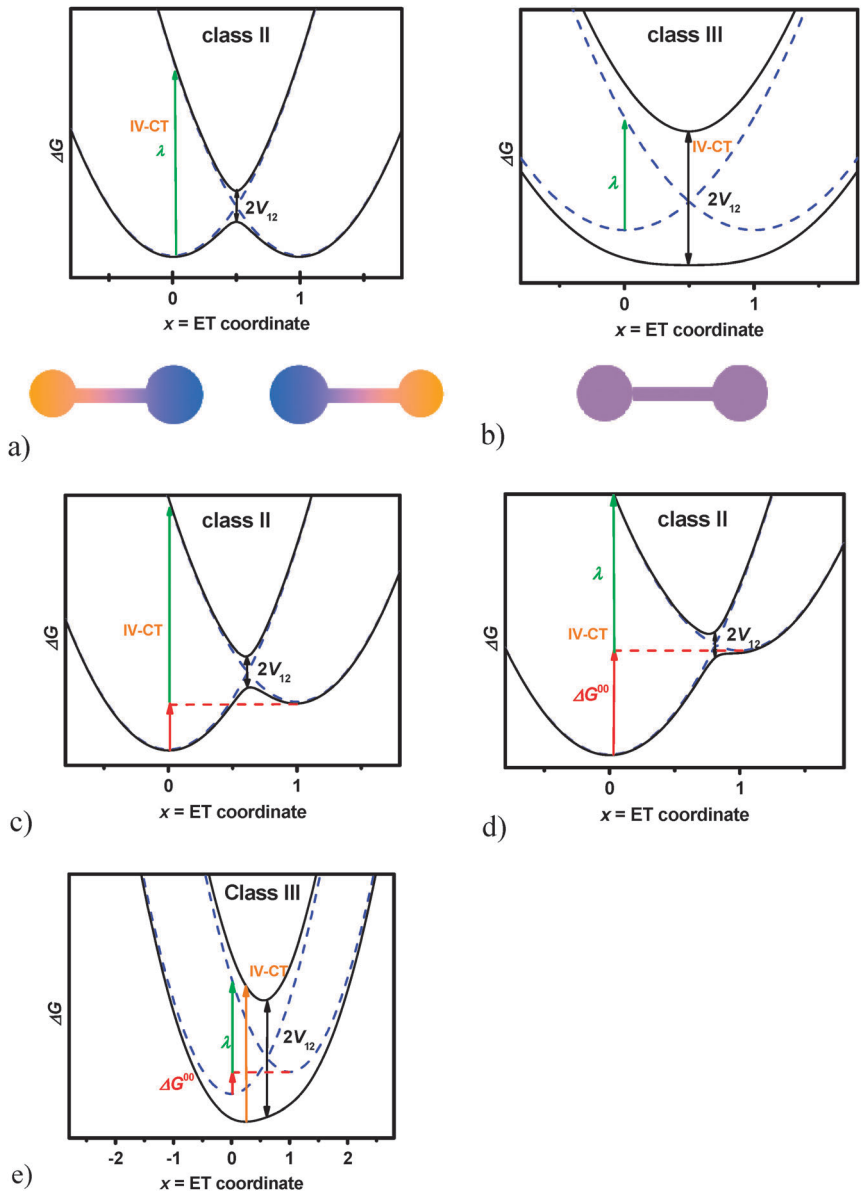

Fig. 1 Calculated (by eqn (1)) diabatic (blue dashed lines) and adiabatic (solid black lines) PESs of class II–III systems with degenerate (a, b) and non-degenerate (c–e) MV systems.

potentials are used for the two diabatic (formally noninteracting) states along an ET coordinate x (Fig. 1).[25–28]

$$\begin{vmatrix} V_{11}-E & V_{12} \\ V_{12} & V_{22}-E \end{vmatrix} = 0 \quad \text{with } V_{11} = \lambda x^2 \tag{1}$$

$$\text{and } V_{22} = \lambda(1-x)^2 + \Delta G^{00}$$

$$V_{12} = \frac{\mu_{ab}\tilde{\nu}_{max}}{\Delta\mu_{12}} \quad \text{with } \tilde{\nu}_{max} = \Delta G^{00} + \lambda \tag{2}$$

$$\mu_{ab}^2 = \frac{3hc\varepsilon_0 \ln 10}{2000\pi^2 N} \frac{9n}{(n^2+2)^2} \int \frac{\varepsilon}{\tilde{\nu}} d\tilde{\nu} \tag{3}$$

$$\Delta\mu_{12} = \sqrt{\Delta\mu_{ab}^2 + 4\mu_{ab}^2} \tag{4}$$

$$\lambda = \lambda_o + \lambda_v \tag{5}$$

where E = eigenvalue, λ = Marcus reorganization energy, x = ET coordinate, ΔG^{00} = free energy difference between the adiabatic ground state (a) and excited state (b), μ_{ab} = transition moment between the adiabatic states, $\tilde{\nu}_{max}$ = absorption maximum of the IV-CT band (= E_{ab}, see below), $\Delta\mu_{12}$ = diabatic dipole moment difference (not experimentally accessible), h = Planck's constant, c = speed of light, ε_0 = permittivity of the vacuum, N = Avogadro's number, n = refractive index of solvent, ε = extinction coefficient, $\Delta\mu_{ab}$ = adiabatic dipole moment difference (measurable by *e.g.* electro-optical absorption spectroscopy), λ_o = outer solvent reorganization energy, λ_v = inner vibrational reorganization energy.

In these secular equations, the two diabatic states 1 and 2 are coupled by the electronic coupling matrix element V_{12} which is a measure for the interaction between the two diabatic redox states (electron mainly located at the one or the other redox center). If we use harmonic potentials for the diabatic

states along the ET coordinate x with the reorganisation energy λ describing the curvature of the potential we obtain an adiabatic double minimum potential if $2V_{12}$ is smaller than λ (Fig. 1a). This is the situation in the bis-triarylamine radical cation **5** which has a large bridge separating the two triarylamine redox centers and which is clearly class II. If $2V_{12}$ is larger than λ, the barrier separating the two minima vanishes and we reach a situation with a single minimum (see Fig. 1b) as is realized in compound **4**, where the two triarylamines share a single phenylene unit. The same holds true if we consider asymmetric MV systems in which the redox centers are inequivalent, for example if different types of redox centers are employed (see Fig. 1c and e). An example is compound **11** which consists of a triarylamine and a perchlorotriphenylmethyl radical redox center (see Chart 2). In this case we have to introduce a free energy difference between the diabatic potentials, ΔG^{00}. A special case arises if ΔG^{00} is as large as λ. In this case the barrier may vanish although $2V_{12}$ is still much smaller than λ (Fig. 1d). In all double minimum cases, an ET process can be optically induced from the ground state to the excited state by excitation into the IV-CT band (Fig. 1a and c).

In the weak coupling regime, where V_{12} vanishes, the maximum of the IV-CT band $\tilde{\nu}_{max}$ corresponds exactly to the sum of the Marcus reorganization energy λ and ΔG^{00} (if present) (Fig. 1a, c and d). The reorganization energy λ can be divided into two terms (eqn (5)): the outer solvent reorganization energy, λ_o, which characterizes the energy needed for the reorientation of the solvent molecules after the ET event and the inner vibrational reorganization energy, λ_v, which is associated with geometrical (bond length and angles) changes of the molecule during ET.

In context of the so-called Generalized Mulliken–Hush theory (GMH)[25,30–32] the parameters describing the ET can be evaluated by analyzing the IV-CT band using eqn (2)–(4).[33–35] In eqn (2), the IV-CT transition moment μ_{ab} can be obtained by integration of the IV-CT band (eqn (3)). The diabatic dipole moment difference $\Delta\mu_{12}$ of the noninteracting diabatic states is needed and can be calculated by eqn (4) from the IV-CT transition moment and the adiabatic dipole moment difference $\Delta\mu_{ab}$. The determination of the latter is thus crucial and can in principle be done by electro-optical absorption (EOA) spectroscopy.[36–41] However, such measurements require high electric fields which cannot be applied to liquid solutions of radical ions as these migrate in the electric field.

Given these fundamental difficulties of a unique experimental discrimination between class II and class III systems in many potentially important cases, a quantum-chemical perspective is highly desirable. However, substantial computational obstacles have prohibited a quantitative description until recently. As the more sophisticated post-Hartree–Fock (HF) *ab initio* methods are computationally too demanding to be applied routinely to the study of realistic organic MV systems,[42,43] the attention so far has centered (a) on density functional theory (DFT) and (b) on semi-empirical MO methods with some type of configuration interaction on top. For reasons explained in more detail below, neither DFT with standard functionals nor the semi-empirical methods were able to reliably and quantitatively describe the molecular and electronic structures of such species in cases when they are close to the class II/III borderline.

We have recently suggested a computational protocol based on hybrid density functionals with a non-standard HF exchange admixture and polarizable continuum solvent models.[29] For a test series of four MV bis-triarylamine radical cations we could show that a computational evaluation of ground- and excited-state properties by this protocol allows a relatively fine bracketing of the localized/delocalized nature, the structure, and the spectroscopic parameters of such systems. In this contribution we will extend the validation of this protocol to a series of bis-triarylamine radical cations with degenerate redox centers which have been well characterized experimentally[5,7,8,10,44–56] and which shall serve as test cases to demonstrate how to apply DFT electronic structure calculations to discriminate between class II and class III MV systems. Furthermore we will apply the same computational protocol[29] to triarylamine-perchlorotriphenylmethyl radical MV systems with non-degenerate redox centers.[57] For the latter series experimental adiabatic dipole moments measured by EOA spectroscopy are available. This is possible because of the neutral character of these MV compounds. Comparison of computed and experimental dipole moments may also serve to illustrate the reliability of our computational protocol.[29]

2. Why the computational characterization is so difficult

Non-DFT-methods

Unrestricted Hartree–Fock (UHF) calculations, either *ab initio* or semi-empirical, tend to give structural symmetry breaking and thus localized charge and spin even in cases that are clearly on the delocalized side. This well-known observation reflects the lack of coulomb correlation, which tends to delocalize charge to a certain extent. Keeping in mind the lack of a clear-cut separation, we may distinguish loosely between non-dynamical correlation, with some near-degeneracy character (but also including the important left-right correlation in chemical bonds), and dynamical correlation that reflects the correlation cusp at small inter-electronic distances. The computational data available so far suggest that both types of correlation need to be taken into account simultaneously for a reliable picture of organic MV systems.

It is known that single-reference perturbation theory, *e.g.* MP2 theory, has difficulties with non-dynamical correlation. Indeed, there have apparently been no serious attempts so far to apply the MP2 method to such organic MV systems. Multi-configuration SCF calculations like, *e.g.*, a complete-active-space SCF (CASSCF) will on the other hand account for the non-dynamical correlation, provided a sufficiently extended active space is employed. Yet the dynamical correlation is missing in this case. Results of the few CASSCF calculations available so far on (relatively small) organic MV systems suggest that these do not sufficiently correct for the tendency of UHF calculations to over-localize.[43,58,59]

A large configuration-interaction or coupled-cluster calculation that takes into account higher-order excitations, or a suitable multi-reference-CI or -perturbation calculation,

accounts for both dynamical and non-dynamical correlation effects. Such methods should thus be adequate. However, when carried out within an *ab initio* framework, their computational cost and unfavorable scaling with system size makes such high-level post-HF calculations currently prohibitive for MV systems of the complexity we are aiming for. With very few exceptions for small models, multi-reference techniques[43] or, for example, CCSD(T) calculations[60] have so far not been applied to the question of symmetry breaking of organic MV systems. Note that a reasonably accurate treatment of the dynamical correlation part (of the correlation cusp) requires the use of rather large one-particle basis sets. This accounts in part for the very large computational effort involved.

Clark and coworkers[61] and others[8,47,62–64] have applied semi-empirical CI calculations to a number of organic MV systems and obtained substantial insights. When applied within a semi-empirical framework, the CI covers mainly the non-dynamical correlation part, whereas it is assumed that the semi-empirical parameterization of the method accounts for the dynamical correlation part (note that semi-empirical MO methods use mainly minimal basis sets and thus could not provide the dynamical correlation explicitly with sufficient accuracy). Obviously, this limits somewhat the scope and quantitative predictive power of the method. The advantage is of course the low computational effort. So far we are not aware of a systematic evaluation of semi-empirical CI methodology for organic MV systems near the class II/III borderline.

DFT methods

DFT methods are currently the workhorse of applied quantum chemistry. They account implicitly for electron correlation, and it is usually assumed that the exchange part of local or semi-local exchange-correlation functionals mimics to a certain extent non-dynamical correlation. Obviously, the accuracy of Kohn–Sham DFT (KS-DFT) depends crucially on the quality of the (approximate) functional. In contrast to the post-HF methods, a systematic improvement of the functional towards an exact theory is not usually achieved (unless one applies the same kind of Hilbert-space expansions of electron correlation as for the former, with a correspondingly unfavorable computational scaling[65–68]). In the context of organic MV systems, so-called self-interaction errors (SIE) are a main obstacle. In contrast to HF theory, most approximate exchange functionals do not correctly cancel the interaction of an electron with its own charge cloud that arises as part of the classical coulomb term of Kohn–Sham theory. The remaining SIE is a serious problem of most contemporary functionals and leads towards too delocalized density or spin-density distributions. In fact, Yang *et al.* have recently introduced and defined a specific "delocalization error" in DFT.[69,70] These problems extend way beyond organic MV systems but are particularly manifest for the latter. As a result, standard functionals with local or semi-local (generalized gradient approximation or related) character will artificially delocalize systems of distinctly localized character provided they are not too far from the class II/III borderline. The latter condition seems to be met for most organic MV systems except for those where the two redox centers are largely de-coupled, *e.g.* by extended saturated spacers. Matters are different for mixed-valence multinuclear transition-metal complexes. In many cases, these seem to be sufficiently localized, in particular for 3d transition-metal systems, so that even GGA functionals provide a well-defined localization of spin on the different metal centers. This is important, in particular in the context of a computational treatment of molecular magnetism or of certain multinuclear metalloenzymes (*e.g.* for iron–sulfur clusters or the multinuclear manganese cluster in photosystem II).

A way to reduce SIE is the inclusion of some amount of exact Hartree–Fock exchange into the exchange functional, replacing some of the (semi-)local exchange. This is done in so-called hybrid functionals. The most popular hybrid functional is the B3LYP functional.[71] As remarked above, HF exchange cancels the coulomb SIE exactly. However, an introduction of 100% exact exchange removes all of the local or semi-local exchange, which before mimicked some of the non-dynamical correlation. The latter would thus have to be reintroduced explicitly, a task that so far has not been solved completely with computationally efficient functionals (see below). Therefore one has to find some compromise between a reduction of SIE and a partial conservation of non-dynamical correlation contributions. In the case of B3LYP this leads to 20% HF exchange and 80% semi-local exchange (with some semi-empirical scaling of the gradient corrections to exchange and correlation). While this seems to provide reasonable thermochemical accuracy for many "normal" systems, the relatively low amount of exact exchange appears to be too low to fully correct the over-delocalization produced by (semi-)local functionals. Our suggested protocol (see below) is thus based on hybrid functionals with enhanced exact-exchange admixture.

Before introducing the approach, it is worthwhile here to also sketch some alternative types of functionals that may in the future solve the problem of a good balance between minimal SIE and introduction of sufficient non-dynamical correlation. We think that a more flexible introduction of exact exchange will be the key to solving this problem, and the functionals in question may be roughly classified as of the hyper-GGA type.[72] One possibility, that has shown promise for spectroscopic calculations within the time-dependent DFT (TDDFT) framework, are the so-called range-separated hybrids, where the exact-exchange admixture to the functional is made dependent on the inter-electronic distance.[73] Alternatively, local hybrid functionals use a position-dependent exact-exchange admixture in real space, governed by a so-called local mixing function.[74] This is an approach currently developed in one of our groups.[75] We should mention furthermore approaches that do indeed start from 100% exact exchange and try to model non-dynamical correlation explicitly in real space. One example for such an approach is Becke's B05 functional.[76,77] Local hybrids may also be reformulated in a similar way.[78,79] Furthermore, specific hyper-GGA functionals have been constructed by Yang *et al.* with an aim to minimize the "delocalization error".[70]

Environmental effects

Apart from the difficulties of including exchange as well as non-dynamical and dynamical correlation in a balanced way and avoiding SIE, we also have to consider other obstacles

that may prevent the accurate computational description of organic MV systems in realistic experimental situations: clearly, environmental effects have to be considered, as most experimental and spectroscopic studies are conducted in a condensed-phase environment. It is clear that the symmetry breaking or charge localization in, for example, a solution or in a crystal will differ from the gas-phase situation. In particular, electrostatic effects will tend to stabilize a charge-localized situation, and in this context a more polar environment will be more effective than a less polar one. Of course, matters are more complex, and solvent polarity is not the only parameter that affects the symmetry breaking. Within a Mulliken–Hush picture (see above), it is the solvent reorganization energy, λ_o, that is a main parameter governing the electron transfer.[23,57,61,64,80–82] A low λ_o will favor a delocalized situation, whereas a larger λ_o will enhance symmetry breaking and move the system towards a class II situation. Notably, a co-existence of localized and delocalized MV systems in the same (intermediate λ_o) solvent has very recently been reported for a dinitro-tolan MV anion.[80]

A full description of microscopic solvation would require dynamical simulations that include both short-range specific solvation as well as long-range dielectric effects. Such simulations are computationally demanding and will currently not be possible for all MV systems of interest. The protocol described below[29] is therefore so far based on a polarizable continuum model. Two types of limitations thus have to be kept in mind:

(a) Even for the ground state, specific solvation effects may be important. Protic solvents are not very common in experimental work on organic MV systems, and we may thus exclude for the moment effects of hydrogen bonding. However, donor–acceptor interactions may become important even for aprotic solvents. For example, it has been argued that dinitroaromatic anions may act as donors towards acceptor solvent molecules like DMSO of DMF.[64] We expect that such specific solute–solvent interactions will be somewhat less important for the bulky triarylamine systems we will discuss mainly in this paper. However, in cationic MV systems, we may not exclude completely that solvent molecules could act as donor towards the solute.

(b) The description of electron transfer, *e.g.* by TDDFT calculations of charge-transfer excitation energies, requires consideration of non-equilibrium solvation. Our suggested protocol uses the non-equilibrium solvation formulation of PCM models by Cossi and Barone,[83] as implemented into Gaussian 03.[84] We will get back to the implications further below.

It is to be expected that environmental effects will be most pronounced when we are dealing with overall charged MV systems. This holds for the bis-triarylamine radical cations studied by us in the first validation study of our computational protocol,[29] and it should hold even more for another well-known class of organic MV systems, the abovementioned dinitro-substituted aromatic radical anions.[61,64,80–82,85–90] In addition to solvent effects, for charged systems interactions with the counter-ions have to be considered. The magnitude of these interactions will depend on (a) the overall delocalization of charge and the size of the delocalization region, (b) potentially on the steric bulk of the MV ion itself that may prevent a closer approach of the counter-ion, (c) the nature and size of the counter-ion (also the question if ion-paired structures or solvent-separated ions are present), and (d) again the cationic or anionic nature of the MV system itself.

3. Computational details

Structure optimizations as well as bonding analyses were performed with a locally modified version of TURBOMOLE 5.9 and 5.10,[91] that allows the exact-exchange admixture in a global hybrid functional to be varied. The "custom hybrid" exchange-correlation functionals were constructed according to eqn (6). In our previous paper,[29] a systematic variation of the exact-exchange coefficient a has been performed, to interpolate between the "pure" gradient-corrected BLYP functional[92,93] ($a = 0.0$) *via* the BHLYP hybrid functional with 50% exact exchange ($a = 0.5$) to a functional made from 100% exact exchange ($a = 1.0$) with LYP correlation[93] on top. In the present work we will focus largely on the optimal value of $a = 0.35$ found in our previous paper. However, we will occasionally also scan larger or smaller values of a, where necessary. In some cases, pure HF calculations without correlation functional have also been performed. SVP basis sets were employed on all atoms[94] (test calculations with larger TZVP basis sets did not change the obtained results noticeably).

$$E_{XC} = (1 - a)(E_X^{LSDA} + \Delta E_X^{B88}) + aE_X^{HF} + E_C^{LYP} \quad (6)$$

In addition to gas-phase optimizations, in all cases optimizations with the COSMO solvent model[95] have been used for hexane ($\varepsilon = 1.89$), for dichloromethane (DCM, $\varepsilon = 8.93$), and for acetonitrile (MeCN, $\varepsilon = 36.64$). Near the critical values of a, where symmetry breaking occurs, the outcome of the structure optimizations depended sometimes on whether we used a symmetrical or unsymmetrical starting structure. In those cases, we therefore tried unsymmetrical starting structures (C_1) as well as symmetrical ones (C_i), as in our previous work. For unsymmetrical cases, this led to a lower energy of the symmetry-broken structure. The electron transfer (ET) barrier was subsequently calculated as the energy difference between the C_i-symmetric transition state and the unsymmetric C_1-optimized minimum. Spin-density isosurface plots were obtained with the Molekel program.[96]

Subsequent TDDFT-calculations of the lowest-energy electronic transitions (IV-CT bands) for both C_1 and C_i structures were done with the Gaussian 03 program,[84] using the same type of custom hybrids and SVP basis sets[94] as discussed above. In the Gaussian 03 calculations, solvent effects have been included by the CPCM keyword, which denotes the polarizable continuum model that is closest to the COSMO model used in the optimizations.[83] Previous test calculations with the more sophisticated IEF-PCM model[97] gave almost identical data.[29] The Gaussian 03 TDDFT results have previously been found to agree better with experiment than the Turbomole data (particularly for symmetrical structures[29]) as soon as a polarizable continuum solvent was included. The differences arise from technical details (van-der-Waals radii, solvent radii, number of tesserae per sphere) in the two solvent-model implementations. In part, the fact that Gaussian 03 but not Turbomole (5.9 or 5.10) includes non-equilibrium solvation in the TDDFT implementation may be responsible. We note in

passing that hybrid functionals with different GGA-type ingredients (*e.g.* PBE exchange and correlation) gave similar ground-state and TDDFT results as the BLYP-based combinations used here.[29] The dipole moments of the first excited states have been calculated by Gaussian 09,[98] using the Gaussian 03 CPCM defaults to reproduce the data of Gaussian 03 calculations.

Hyperfine coupling (HFC) constants have been calculated by generating the Kohn–Sham orbitals using Turbomole, with IGLO-II basis sets (H (3s1p)/[5s1p], C N O (5s4p1d)/[9s5p1d])[99] and the hybrid functional including 35% (a = 0.35) exact exchange admixture. The orbitals were then transferred to our in-house MAG-ReSpect program package[100] for computation of the HFCs.

4. Molecular test set

Our previous validation[29] focused on the four bis-triarylamine radical cations **1–4** (Chart 1). These four MV radical cations contain two *N*,*N*-di(4-methoxyphenyl)-moieties as redox centers with different bridge units of decreasing length from **1** to **4**. They are all close to the class II/III borderline but represent a fairly good range of situations starting from **1**, which is most clearly on the localized class II side in a polar solvent *via* **2**, which is still just on the class II side, **3**, which is just class III and **4** which is clearly class III. Notably, the calculations classified all four systems as class III in a hexane solvent model, but the protocol gave a rather good representation in the more polar solvents MeCN and DCM, which represent realistic solvents used experimentally (the radical cations tend to be insoluble in nonpolar solvents). Here we extend the validation to the larger set of bis-triarylamine radical cations **5–10** (Chart 1), and to the unsymmetrical neutral triarylamine-perchlorotriphenylmethyl radicals **11–17** (Chart 2). The systems **5–8** may be derived from **1** by inserting different aryl groups into the center of the bridge. In **5** this is an unsubstituted phenyl group. The electron richness increases *via* the 2,5-dimethyl-substituted **6** to the 2,5-dimethoxy-substituted **7** to **8**, where an anthracene group is at the center of the bridge. It may be assumed that the increasingly electron-rich aryl groups will successively enhance the coupling between the two triarylamine units and thus move the character towards class III. This is confirmed by

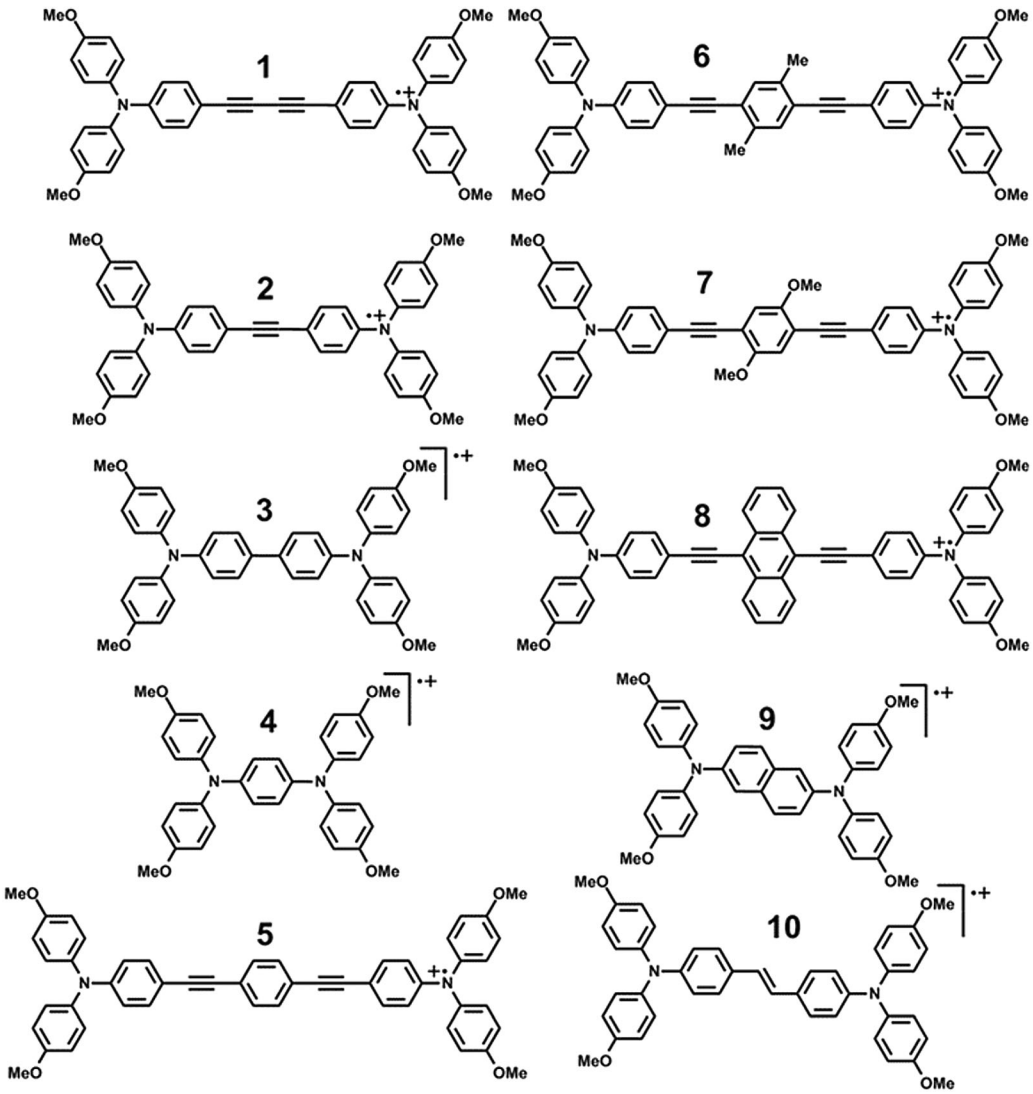

Chart 1 MV bis-triarylamine radical cations used for validation (cations **1–4** have already been employed in ref. 29).

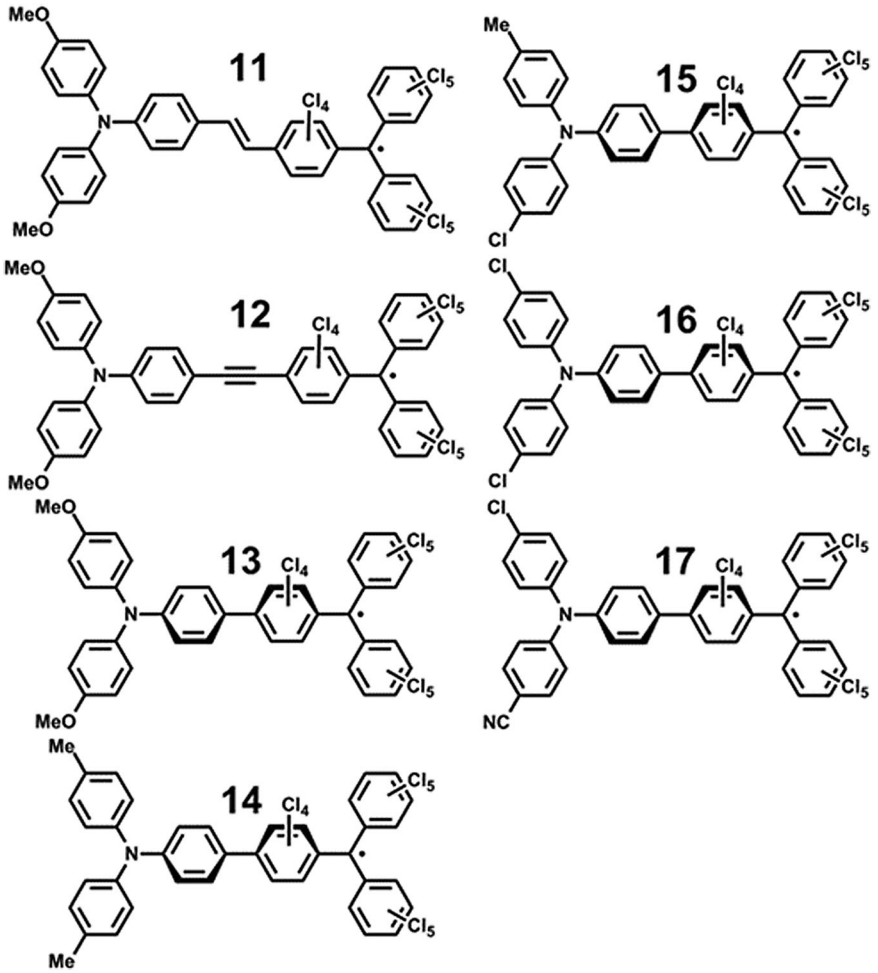

Chart 2 Neutral MV systems **11–17**.

experimental observations (see below).[5,7,8,10,44–52] Cation **8** exhibits the rather large central anthracene group and thus is a special case (see below).[8] Cations **5–7** move towards the border from the class II side. Compound **8** is particularly close to the border, as exemplified by the spectroscopic observation of a class II behavior in MeCN and a class III behavior in DCM.[8] Finally, **9** and **10** have relatively short bridges and are expected to be on the class III side.[5,44,47,49,53–56]

The radicals **11–17** are asymmetric neutral mixed-valence systems with two inequivalent redox centers. However, they have an electronic structure closely related to the bis-triarylamine radical cations and feature a number of interesting properties that make them suitable targets for further study. While **11** and **12** possess an ethylene and an acetylene moiety in the center of the bridge, compounds **13–17** have a direct biphenyl connection, but different substitution patterns. While they all feature a perchlorinated triphenylmethyl radical (PCTM) acceptor group, the substituents in *para*-position of the two terminal aryl groups of the triarylamine donors change from two methoxy (**13**) *via* two methyl (**14**) *via* methyl/chloro (**15**), two chloro (**16**) to chloro/cyano (**17**) groups (Chart 2). These small substituents influence the electron donor strength of the triarylamine, that is, the triarylamine in **13** is the strongest donor while that of **17** is the weakest. Thus, this series allows for the investigation of subtle donor–acceptor strength variations. Due to their neutral character, it is expected that solvent effects may be less pronounced for radicals **11–17** than for the cations **1–10**. The first experimental studies on such unsymmetrical compounds have been carried out recently,[57,101] with particular emphasis on **11**, **12** and **13**. As the donor is clearly on the triarylamine side, these systems are best represented as localized class II cases, possibly with only one minimum along the ET coordinate. We will focus our attention in particular on their IV-CT band.

5. Results and discussion

Bis-triarylamine radical cations, ground-state properties

Table 1 summarizes the key ground-state parameters of **5–10** computed using 35% HF exchange admixture, for DCM and MeCN solvent models (results in cyclohexane or in the gas phase place **1–10** generally on the delocalized class III side; data not shown). This allows us to see whether our protocol established successfully for **1–4** is useful also for the remaining six cations. We find **5–7** to be localized (class II) in both solvents, in agreement with experimental observation.[5,7,8,10,44–52] This is indicated by the ET barriers, the dipole moments, and the

Table 1 Calculated key ground state parameters for **5–10**.[a] Total dipole moment μ_a, enthalpy ΔH^* as energy difference between computed C_i and C_1 symmetrical structures, spin expectation value $\langle S^2 \rangle$ (theoretical value would be 0.75), key distance C_{Ar}–N between the nitrogen atom and the carbon atom of the outer phenyl ring, as well as the ^{14}N-HFC constants a_N at the two nitrogen atoms

Molecule in solvent	μ_a/D[b]	ΔH^* (C_i – C_1)/kJ mol^{-1}	$\langle S^2 \rangle$	C_{Ar}–N/Å	a_N/MHz	a_N/MHz
					C_1	C_i
5 in DCM	40.2	10.02 (12.6[c]/13.9[c])	0.79	1.406	24.4 (23.5)[c]	10.6
				1.426	0.3	10.6
5 in MeCN	42.1	15.64	0.79	1.405	24.6	10.7
				1.426	0.2	10.7
6 in DCM	38.9	4.77 (10.8)[c]	0.79	1.407	24.0 (23.1)[c]	10.1
				1.426	0.4	10.1
6 in MeCN	41.2	10.27 (5.7)[d]	0.79	1.405	24.6	10.2
				1.426	0.2	10.2
7 in DCM	35.2	3.09 (6.9)[e]	0.79	1.412	22.4	7.9
				1.425	0.8	7.9
7 in MeCN	40.0	8.35	0.79	1.408	24.2	7.8
				1.425	0.3	7.8
8 in DCM	0.0	0.32 (0.0)[e]	0.78	1.430	5.9	5.9
				1.429	5.9	5.9
8 in MeCN	0.0	0.46	0.78	1.430	5.7	5.7
				1.430	5.7	5.7
9 in DCM	0.8	−0.04	0.77	1.426	14.6	14.1
				1.425	13.6	14.1
9 in MeCN	0.7	0.05	0.77	1.426	14.5	14.1
				1.425	13.7	14.1
10 in DCM	0.1	0.27	0.77	1.429	10.4	10.6
				1.429	10.5	10.6
10 in MeCN	0.1	0.29	0.77	1.429	10.2	10.3
				1.429	10.3	10.3

[a] With 35% HF exchange and COSMO. Experimental values in parentheses. Further computational data are available in Tables S5–S10 in ESI.† [b] With the center of mass as the origin. [c] ΔH^* by EPR spectroscopy, ref. 46. [d] Ref. 52. [e] ΔG^* from a fit of the potential energy surface to the experimental absorption spectra, ref. 8.

asymmetry of the C_{Ar}–N distances. As expected from the increasing donor capacity of the substituents on the central phenyl ring (H for **5**, CH_3 for **6**, and OCH_3 for **7**), the amount of symmetry breaking tends to decrease from **5** to **7** in a given solvent (albeit **5** and **6** behave very similarly and only **7** is notably less localized). The more polar MeCN is moreover expected to give rise to a more pronounced symmetry breaking compared to DCM. The slightly lower ET barrier of **6** compared to **5** in DCM is consistent with the barriers estimated experimentally (by temperature-dependent EPR, see below).[46] The fact that **7** has the lowest ET barrier (as well as dipole moment and structural asymmetry, Table 1), is also consistent with the lower end of the range of measured ET barriers, but the experimental uncertainty is higher in this case.[8]

The ET barriers for **5–8** in MeCN and DCM are graphically compared in Fig. 2. The increase of the donor capacity of the substituents from **5** to **8** leads to a decrease of the ET barriers. The ET barriers in DCM are about 5 kJ mol^{-1} lower than the barriers in MeCN, as expected. Compared to experimental results in DCM, the ET barriers computed in the same solvent are underestimated. Curiously, the values computed for MeCN tend to be closer to the experimental DCM data.

The ^{14}N-HFC constant for **5** in DCM is found to be 23.5 MHz (0.839 mT) experimentally[46] and 24.4 and 0.3 MHz, respectively, using 35% of HF exchange admixture (see Table 1). The computed HFC constant for **6** (about 24.0 MHz in DCM) agrees also well with the measured one (23.1 MHz) and confirms the class II character.[46] This suggests the computed HFC constants (22.4 MHz in DCM) for the related **7**, where

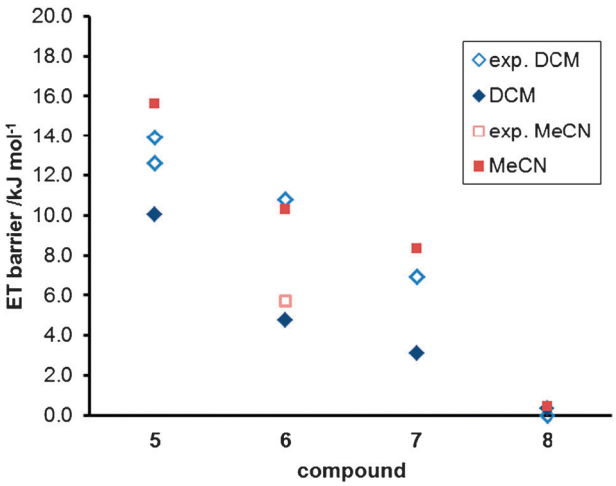

Fig. 2 Computed ET barriers ΔH^* of **5–8** in DCM (dark blue, ◆) and MeCN (dark red, ■) compared to experimental values according to Table 1 (light colored, ◇ and □). Two different experimental results for **5** in DCM are obtained either by EPR spectroscopy (larger value, ref. 46), or from a fit of the potential energy surface to the experimental absorption spectra (lower value, ref. 8).

no experimental data are available, to also be reliable. The somewhat lower HFC points to increased delocalization in **7**, comparable to trends in the class II systems with HFC constants of 23.3 MHz for **1** in DCM (see Table S1 in ESI†) and 17.0 MHz for **2** (Table S2, ESI†). The calculated values indicate **2** to be a system very close to the class II/III

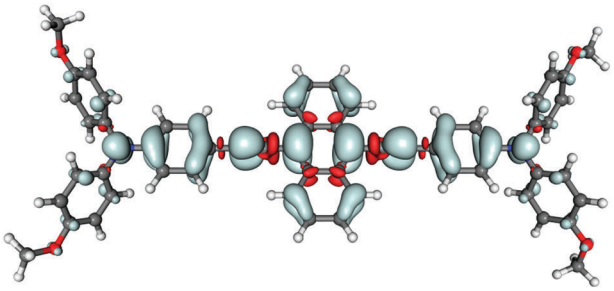

Fig. 3 Spin density isosurface plot (±0.001 a.u.) for **8** in MeCN showing substantial spin delocalization onto the anthracene bridge.

borderline: in the localized case, one expects one HFC constant near 20 MHz, the other vanishing. Two identical HFC constants of about 10 MHz are expected for true class III systems. The decisive evidence for **2** being class II was, however, the comparison of the coupling matrix element $2V_{12} = E_{ab}$ (C_i) with the calculated excitation energy of the transition state.[29]

Cation **8** may be viewed as a further extension of the series **5–7**, as it exhibits the most electron-rich aryl moiety in the middle of the bridge, an anthracene unit (Chart 1). As mentioned above, **8** is particularly close to the class II/III border and appears to switch from class II to class III simply by changing the solvent from MeCN to a solution of 5% MeCN in DCM, as indicated by UV/vis data.[8] Optimization with 35% HF exchange admixture in COSMO solvent models for MeCN and DCM gives generally a delocalized class III situation (negligible dipole moment, ET barrier, structural distortion and nonequivalence of the HFCs). This indicates that this compound may probe the limits of the suggested protocol. Symmetry breaking may be induced by either (a) increasing exact-exchange admixture to 40% in MeCN, or alternatively by (b) increasing the dielectric constant of the model solvent from $\varepsilon = 36.64$ for MeCN to $\varepsilon = 50$. But even then no noticeable ET barrier has developed (indeed, the delocalized structure remains slightly more stable). Only a pure HF calculation without correlation functional provides a sizeable ET barrier (156.9 kJ mol^{-1}) and a clearly localized description (but with sizeable spin contamination). Apart from the fact, that this compound is probably the one closest to the class II/III borderline of all compounds studied so far, its large aromatic anthracene unit in the center of the bridge may also represent a challenge to the continuum solvent model used. It is conceivable that direct solvent coordination to the electron-rich aromatic ring may be involved, which is not covered by the model (Fig. 3 clearly shows the substantial spin delocalization onto the anthracene moiety which also leads to comparatively small ^{14}N-HFC constants). A treatment that includes the actual solvent dynamics explicitly is outside the scope of this study. Compound **8** remains thus a veritable challenge.

On the other hand, compounds **9** and **10**, with their rather short bridges, exhibit large coupling of the two redox centers, almost as found for **4** (see above). Consequently, they are both classified as delocalized, symmetrical class III systems by our protocol (*cf.* data in Table 1, Table S9–S10 in ESI†), consistent with experimental evidence from IV-CT line shape and solvatochromism, crystallography and vibrational spectra.[47,49]

Table 2 Computed IV-CT transition energies E_{ab} and transition moments μ_{ab} for **5–10** in DCM and MeCN compared to available experimental data (in parentheses)

Molecule in solvent	E_{ab}/cm^{-1} C_1[b]	E_{ab} (=$2V_{12(two\text{-}state)}$)[a]/cm^{-1} C_i[c]	μ_{ab}/D C_1	μ_{ab}/D C_i	Ref.
5 in DCM	6969	2421 *[1896]*[d]{2087}[f]	10.62	35.46	
	(8060)	(2000)[e]	(6.2)		7, 8
	(7780)		(5.85)		47, 49
5 in MeCN	8351	2654 *[2003]*[d]{2282}[f]	9.15	33.49	
	(9910)				47
6 in DCM	6828	2537 *[2068]*[d]{2280}[f]	11.60	34.74	
	(7500)	(2440)[e]	(7.6 ± 0.3)		10
6 in MeCN	8150	2847 *[2125]*[d]{2439}[f]	9.81	32.78	
7 in DCM	6000	3969 *[2543]*[d]{3260}[f]	15.66	28.82	
	(6520)	(3820)[e]	(9.7)		7, 8
7 in MeCN	7436	4184 *[2428]*[d]{3214}[f]	12.04	27.86	
8 in DCM[g]	5881	5844 *[5881]*[d]{5857}[f]	22.27	22.36	
		(4640)		(14.1)	8
8 in MeCN[g]	6127	6054 *[6127]*[d]{6079}[f]	21.40	21.57	
	(6770)				8
9 in DCM[g]	7891	7874 *[7866]*[d]{7869}[f]	14.19	14.23	
		(7620)		(11.1)	5
9 in MeCN[g]	8065	8166 *[8043]*[d]{8112}[f]	13.90	13.82	
10 in DCM[g]	7211	6959 *[7211]*[d]{7086}[f]	18.18	18.50	
		(6150)		(13.0)	53
		(6080)		(13.5)	47
10 in MeCN[g]	7661	7390 *[7661]*[d]{7523}[f]	17.40	17.72	
		(7010)			47

[a] This equivalence holds only within the two-state model. [b] Computed excitation energies in C_1-symmetry compared to maximum absorption in UV/vis spectra in parentheses, where available. [c] Computed excitation energies in C_i-symmetry compared to "experimental" $2V_{12}$ from the two-state model in parentheses, where available. [d] $2V_{12}$ in italics and brackets obtained alternatively from computed dipole moments and excitation energies *via* eqn (2) and (4). [e] Experimental coupling $2V_{12}$ evaluated by a three-state Mulliken–Hush-analysis. [f] Evaluated by eqn (2) and $\Delta\mu_{12} = 2\mu_{ab}(C_i)$. [g] In these cases differences between the C_1 and C_i structure is marginal which thus leads to identical E_{ab} values.

Bis-triarylamine radical cations, IV-CT transition

Table 2 summarizes the excitation energies and transition moments computed by TDDFT methods for **5–10**, in comparison with the available experimental data.

For **5**, the computed excitation energy of 6969 cm^{-1} in DCM deviates by about 1000 cm^{-1} from the recently obtained experimental data.[8,46,49] The computed electronic coupling $2V_{12} = E_{ab}(C_i)$ in DCM agrees within 400 cm^{-1} to experimental estimates within a two-state model.[8,46] For **6**, the computed IV-CT excitation energy in DCM model solvent lies within 700 cm^{-1} from experiment[10,46] and the computed electronic coupling $2V_{12}$ agrees excellently (within better than 200 cm^{-1}) to the experimentally obtained value.[10] Similar agreement with experiment is found for **7**, with a deviation of only about 520 cm^{-1} for the IV-CT band and of about 150 cm^{-1} for $2V_{12}$.[8]

In case of **8**, the computations underestimate the excitation energy in MeCN by 650 cm^{-1}, that in DCM by 1200 cm^{-1}.[8] For all these comparisons one has to keep in mind that twice the computed electronic coupling refers to the energy difference of ground and excited state at C_i geometry (which is exact in a two-state one-mode model with harmonic potentials as given in Fig. 1) while the experimental couplings were estimated by a three-state generalized Mulliken–Hush model. In cases where the third state plays a minor role, this comparison is reasonable. However, for **8** in DCM, a class III system with strong mixing of states, this comparison is no longer useful. In this case one can simply take the IV-CT energy as twice the coupling as given in Table 2.

Turning to the more clearcut class III cases **9** and **10**, we see very good agreement with experiment of excitation energy and transition moment computed for **9** in DCM.[5] For **10**, we see an overestimate of the measured IV-CT excitation energy[47] by 1100 cm^{-1} in DCM and by 650 cm^{-1} in MeCN.

The computed transition and dipole moments of ground and excited state allowed us also to calculate $2V_{12}$ by eqn (2) and (4) by using purely DFT computed input. As can be viewed from Table 2 the agreement with DFT computed E_{ab} is generally reasonable for localized **5–7** and excellent for delocalized **8–10** in both solvents. An alternative way to compute $2V_{12}$ by Eqn (2) follows an idea of Matyushov and Voth[102] and of Coropceanu *et al.*[20] who showed that the diabatic transition dipole moment difference is equal to twice the adiabatic transition moment ($\Delta\mu_{12} = 2\mu_{ab}(C_i)$) at the transition state of the thermal ET within the two-level model. The $2V_{12}$ values computed in this way proved to be in better agreement with computed E_{ab} for the localized set of compound while they are equally excellent for the delocalized set.

Overall, it appears that the computed transition moments correlate well with the experimental ones but overestimate the latter consistently. As seen in Fig. 4, the transition dipole moments increase when moving towards class III character, due to the better overlap of the ground and excited state wave functions in delocalized systems.

Fig. 5 displays graphically the agreement with experiment of IV-CT excitation energies for **1–10** in DCM computed using the present protocol. Apart from the overall very satisfactory agreement, we note in particular that we seem to systematically underestimate somewhat the excitation energies for the class II systems (**1**, **2**, **5**, **6**, **7**), whereas we overestimate them for the clearcut class III systems (**4**, **9**, **10**), particularly for **10**. The borderline class III case **3** is well described,[29] whereas the difficulties in describing the extremely subtle situation for the extreme borderline case **8** are reflected by a relatively large overestimate.

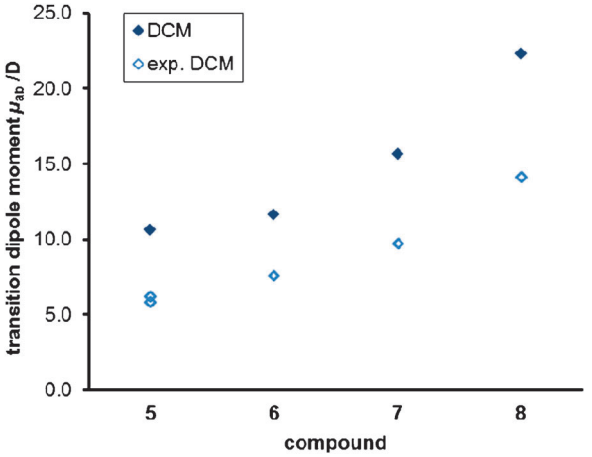

Fig. 4 Computed transition moments of **5–8** in DCM (dark blue, ◆) compared to experimental values (light blue, ◇) according to Table 2.

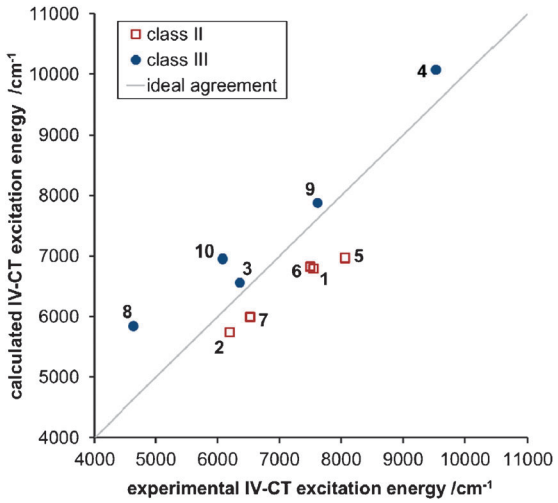

Fig. 5 Comparison of IV-CT excitation energies computed for **1–10** with experimental data (computations with 35% HF-like exchange in DCM for structure and TDDFT calculation, experimental data in DCM).

Neutral perchlorotriphenylmethyl-triarylamine radicals

Turning now to the application of the computational protocol to the unsymmetrical, neutral radicals **11–17** (Chart 2), our focus below will be on the comparison of the computed IV-CT band and dipole moments with experiment. We first note that the optimized ground-state structures, which have been computed with our usual protocol (35% HF exchange admixture in DCM COSMO solvent), reflect the localized electronic structure of the radicals, which have their spin density predominantly on the perchlorotriphenylmethyl

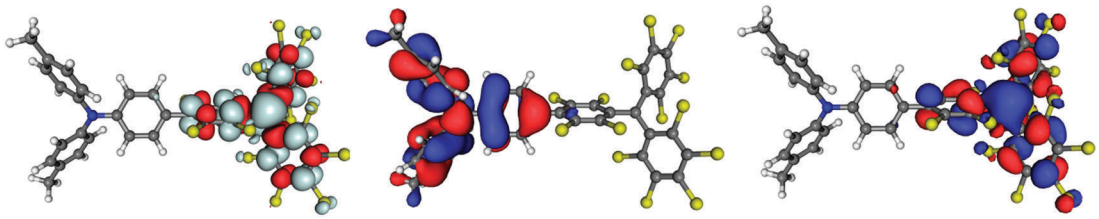

Fig. 6 Ground-state electronic structure for **14** (at 35% HF exchange in hexane). Left: spin density (isovalue ±0.001 a.u.). Middle: β-HOMO (isovalue ±0.02 a.u.). Right: β-SOMO (isovalue ±0.02 a.u.).

(PCTM) radical center, as expected (Fig. 6; structural data are summarized in Table S19 in ESI†). This is also indicated by the ^{13}C HFC constants, which are calculated (35% HF exchange in MeCN, DCM and hexane) to be 96–97 MHz for **11** and **12** (with a weak dependence on exact-exchange admixture), consistent with experimental values of about 84 MHz for the PCTM radical (obtained by EPR spectra in THF and tetrachloroethylene).[103] Consequently, the IV-CT band is expected to correspond to an excitation from the triarylamine to the PCTM radical moiety, as confirmed by the character of the HOMO and SOMO (Fig. 6) and by the analysis of the TDDFT data. Calculations on different diastereomers of **14** and **17** do not change the results noticeably.

The calculations confirm the doublet character of the ground state and of the first excited state (the "IV-CT" state). Computations in DCM place the first quartet state at 16 436 cm^{-1}, 18 547 cm^{-1} and 22 439 cm^{-1} above the ground state for **11**, **12**, and **17** respectively.

Straightforward application of our TDDFT protocol with 35% HF exchange to the IV-CT excitation energies provides a systematic overestimate compared to experiment[57] of about 2000–2500 cm^{-1} for **11–13**, and of about 2700–3500 cm^{-1} for **14–17** (Table 3, Fig. 6). The same types of calculations produced much closer agreement with experiment for the cationic bis-triarylamines (see ref. 29 and Table 2). We may reduce this overestimate notably by reducing the HF exchange admixture to 30% (Table 3): now deviations are about 700–1500 cm^{-1} (test calculations indicate that at 25% the computed energies are already underestimated somewhat). Why is less exact-exchange admixture required for the neutral radicals **11–17** than for the cations **1–10**? It appears possible, that the HF exchange admixture of 35% found to be optimum for both ground- and excited-state calculations on the cationic species may have compensated for some counterion effects neglected in the computational protocol. As these are absent for the neutral radicals, less exact exchange is required. Due to the unsymmetric, localized character of **11–17**, we could not probe at which exact-exchange admixture a delocalized ground-state situation would occur for these systems.

While UV/vis data for **14–17** are available only in cyclohexane (computations were done with $\varepsilon = 1.89$ for hexane, which is only a minor difference to $\varepsilon = 2.02$ of cyclohexane), data for cyclohexane, MeCN, and DCM are available for **11–13** (see above). The calculations confirm essentially the somewhat larger excitation energy in (cyclo-)hexane compared to DCM. But they would suggest essentially no differences between DCM

Table 3 Computed and experimental lowest excitation energies E_{ab} and transition moments μ_{ab} for **11–17**, depending on solvent and on exact exchange admixture in TD-DFT functional

		E_{ab}/cm^{-1}			μ_{ab}/D		
Compound	Exact exchange admixture	Hexane	DCM	MeCN	Hexane	DCM	MeCN
11 (stilbene)	exp.[a]	12 400	12 150	12 200	3.6		3.6
	30%	13 189	12 956	12 940	5.1	5.2	5.2
	35%	14 539	14 392	14 394	4.2	4.4	4.4
12 (acetylene)	exp.[a]	12 650	12 300	12 450	4.1		4.1
	30%	13 626	13 435	13 390	6.0	6.1	6.1
	35%	14 904	14 782	14 745	5.2	5.3	5.3
13 (OMe/OMe)	exp.	12 700[b] 13 200[a]	13 150[a]	13 450[a]	1.21[b]		
	30%	13 715	13 618	13 669	2.5	2.5	2.4
	35%	15 812	15 731	15 796	2.4	2.4	2.3
14 (Me/Me)	exp.[b]	13 150			1.23		
	30%	14 674	14 463	14 457	2.2	2.3	2.2
	35%	16 735	16 534	16 545	2.2	2.3	2.1
15 (Me/Cl)	exp.[b]	14 400			1.31		
	30%	15 646	15 351	15 288	2.0	1.9	2.0
	35%	17 743	17 471	17 407	1.9	1.9	1.9
16 (Cl/Cl)	exp.[b]	15 100			1.16		
	30%	16 568	16 167	16 092	1.8	1.8	1.7
	35%	18 674	18 304	18 244	1.9	1.8	1.7
17 (Cl/CN)	exp.[b]	17 400			1.17		
	30%	18 348	18 031	18 118	2.1	1.7	1.1
	35%	20 274	20 095	20 281	2.1	1.8	1.2

[a] Experimental values from ref. 57. [b] Experimental values in cyclohexane from ref. 101.

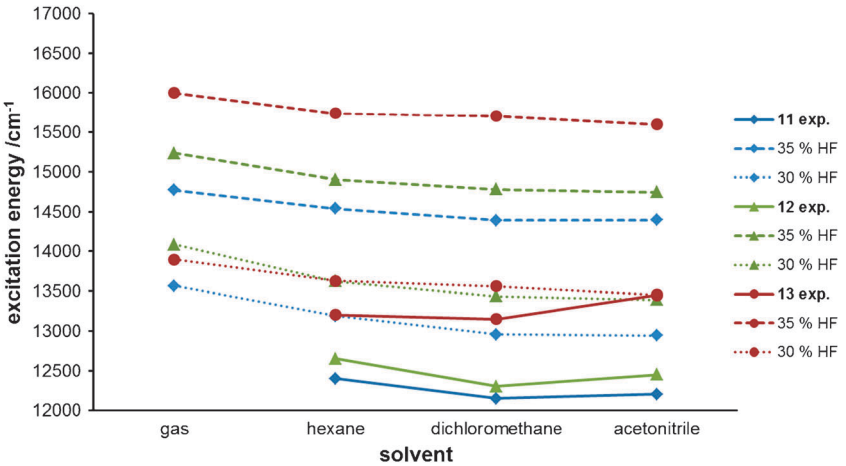

Fig. 7 Excitation energies for **11**, **12**, and **13**, computed by TDDFT for different exact-exchange admixtures and for different solvents. Experimental data are connected by solid lines, computational ones by dashed (35% HF exchange) or dotted (30% HF exchange) lines.

Table 4 Experimental ground-state dipole moment μ_a, dipole moment difference $\Delta\mu_{ab}$ between ground and Franck–Condon excited-state ($\Delta\mu_{ab} = \mu_b - \mu_a$) and electronic coupling V_{12} for **13–17** from electro-optical absorption spectroscopy in cyclohexane at 298 K. Computed ground-state dipole moments in parentheses (plot of calculated dipole moments, see Fig. S2, ESI†)

	13 (OMe/OMe)	**14** (Me/Me)	**15** (Me/Cl)	**16** (Cl/Cl)	**17** (Cl/CN)
μ_a/D	4.6 ± 0.6 (3.2[a])	4.6 ± 0.2 (3.8)	3.2 ± 0.2 (3.1)	2.5 ± 0.2 (0.5)	0.3 ± 0.4 (−4.4[b])
$\Delta\mu_{ab}$/D	30.7 ± 6.9	28.4 ± 1.6	28.5 ± 1.4	28.8 ± 1.7	26.5 ± 2.7
V_{12}/cm^{-1}	500	570	660	620	770

[a] This is the dipole moment of the C_2-symmetric structure. It is 5.2 D for the isoenergetic non-symmetric structure (rotated methoxy-groups). [b] The change in sign indicates that the direction of the dipole moment vector has reversed. This cannot be probed by electro-optical absorption spectroscopy.

and MeCN, whereas experimentally there is a somewhat larger difference for **13** (Table 3, Fig. 7).

Transition dipole moments μ_{ab} for **11–17** were systematically overestimated by the computations (Table 3). But they are strongly dependent on rotations around the biphenyl axis. With the two phenyl groups orthogonal, the transition dipole moment almost vanishes, due to the small overlap of the π-orbitals. The computed potential energy surface for this rotation is extremely flat, and a dynamical situation is likely, rendering the computed transition dipole moments less well defined.

Ground-state dipole moments μ_a and dipole moment differences $\Delta\mu_{ab}$ for **13–17** have been determined by electro-optical absorption spectroscopy in cyclohexane at 298 K (Table 4, Table S18, ESI†). They decrease along the series **13–17** as the substituents attached to the triarylamine are less electron donating/more electron withdrawing. For **17** the ground-state dipole moment almost vanishes. Agreement between computation and experiment is qualitatively reasonable for these neutral systems, where dipole moments are well defined. However, the decrease of computed values from **13** to **17** is more pronounced than the experimental decrease, leading to a vanishing moment already for **16** and to an inversion of the direction for **17**. The direction is essentially towards the PTCM side for **13–15** and to the opposite side for **17** (see Fig. S2, ESI†). While for the species with C_2 symmetry the computed ground-state dipole moments point exactly along the long molecular axis between the nitrogen atom and the carbon atom (see Table 4), those with C_1 symmetry (**15**, **17**) display stronger deviations. This is particularly so for **17** where the local dipole moment of the aminobenzonitrile chromophore within the triarylamine breaks the symmetry and reverses the overall ground-state dipole moment. The torsion angle around the biphenyl axis is around 70° for **13–17**, depending only slightly on the polarity of the solvent. This twisting contributes to a partial decoupling of the two redox centers and affects the excitation energies and transition moments substantially (see for example Table S14 in ESI† for **14**). The dynamics of this rotation should thus be kept in mind regarding the agreement of the TDDFT results with experiment. On the other hand, the electronic coupling V_{12} evaluated by eqn (2) and (4) depends only moderately on the substituents.

6. Conclusions and outlook

The validation of a recently introduced computational protocol for the computational description of organic mixed-valence compounds based on non-standard hybrid functionals and continuum solvent models has been extended to a larger number of compounds, including ten cationic bis-triarylamine radical cations and seven neutral triarylamine-triarylmethyl radicals. The latter neutral radicals are of substantial interest in their own right and have been evaluated also in detail experimentally.

Performance of the protocol for the newly included cationic radicals **5–10** is comparable to the previously obtained results for the cations **1–4**. This holds for the ground-state properties

as well as for the IV-CT bands. That is, the localized class II *vs.* delocalized class III character of these mixed-valence systems is reproduced well by the protocol, provided that the polar solvent is included by a continuum model. Rather accurate IV-CT excitation energies and transition dipole moments may also be obtained computationally. The limits of the suggested protocol are probed by compound **8**. This cation is so close to the class II/III borderline, that experimentally a change of solvent from acetonitrile to dichloromethane switches the situation from class II to class III. The protocol with 35% HF exchange admixture does not recover this switch but would predict the system as class III in both solvents. It appears possible that the presence of a large anthracene aromatic ring system at the center of the bridge in **8** gives rise to specific solvent effects that are not included in the current model.

In case of the neutral radicals **11–17**, the protocol does seem to provide a good description of the ground-state properties (*e.g.* dipole moments). However, the lowest excitation energies are overestimated by about 2000–3500 cm^{-1} when using 35% HF exchange admixture. A reduction to 30% brings computations into better agreement with experiment. We speculate that the larger exact-exchange admixture needed to give sufficient symmetry breaking for class II cationic systems may compensate to some extent for counterion effects not present in the model. As these are absent in the neutral radicals, slightly less exact-exchange admixture is adequate for their description.

It thus seems that the greatest remaining challenge in the computational evaluation of organic mixed-valence systems is the proper description of environmental effects. Inclusion of specific solvation and of counterion effects (for ionic species) will require modifications to our model, which we currently examine, together with overall more satisfactory DFT functionals. However, even at the present stage, the model allows a considerably more realistic computational study of such mixed-valence systems than hitherto possible.

Acknowledgements

This work has been supported by Deutsche Forschungsgemeinschaft within Graduiertenkolleg 1221 "Control of electronic properties of aggregated π-conjugated molecules". M.R. is grateful to Bayerische Eliteförderungsgesetz for a PhD scholarship.

References

1 B. S. Brunschwig, C. Creutz and N. Sutin, *Chem. Soc. Rev.*, 2002, **31**, 168–184.
2 J.-P. Launay, *Chem. Soc. Rev.*, 2001, **30**, 386–397.
3 P. Chen and T. J. Meyer, *Chem. Rev.*, 1998, **98**, 1439–1477.
4 S. F. Nelsen, R. F. Ismagilov and D. A. Trieber, *Science*, 1997, **278**, 846–849.
5 C. Lambert and G. Nöll, *J. Am. Chem. Soc.*, 1999, **121**, 8434–8442.
6 C. Lambert, G. Nöll and F. Hampel, *J. Phys. Chem. A*, 2001, **105**, 7751–7758.
7 C. Lambert, G. Nöll and J. Schelter, *Nat. Mater.*, 2002, **1**, 69–73.
8 C. Lambert, S. Amthor and J. Schelter, *J. Phys. Chem. A*, 2004, **108**, 6474–6486.
9 C. Lambert, C. Risko, V. Coropceanu, J. Schelter, S. Amthor, N. E. Gruhn, J. C. Durivage and J.-L. Brédas, *J. Am. Chem. Soc.*, 2005, **127**, 8508–8516.
10 S. Amthor and C. Lambert, *J. Phys. Chem. A*, 2006, **110**, 1177–1189.
11 V. Lloveras, J. Vidal-Gancedo, D. Ruiz-Molina, T. M. Figueira-Duarte, J.-F. Nierengarten, J. Veciana and C. Rovira, *Faraday Discuss.*, 2006, **131**, 291–305.
12 C. Rovira, D. Ruiz-Molina, O. Elsner, J. Vidal-Gancedo, J. Bonvoisin, J.-P. Launay and J. Veciana, *Chem.–Eur. J.*, 2001, **7**, 240–250.
13 J. Sedo, D. Ruiz, J. Vidal-Gancedo, C. Rovira, J. Bonvoisin, J. P. Launay and J. Veciana, *Adv. Mater.*, 1996, **8**, 748–752.
14 S. F. Nelsen, R. F. Ismagilov and D. R. Powell, *J. Am. Chem. Soc.*, 1997, **119**, 10213–10222.
15 S. F. Nelsen, A. E. Konradsson and Y. Teki, *J. Am. Chem. Soc.*, 2006, **128**, 2902–2910.
16 D. L. Sun, S. V. Rosokha, S. V. Lindeman and J. K. Kochi, *J. Am. Chem. Soc.*, 2003, **125**, 15950–15963.
17 S. V. Lindeman, S. V. Rosokha, D. L. Sun and J. K. Kochi, *J. Am. Chem. Soc.*, 2002, **124**, 843–855.
18 S. F. Rak and L. L. Miller, *J. Am. Chem. Soc.*, 1992, **114**, 1388–1394.
19 T. H. Jozefiak, J. E. Almlof, M. W. Feyereisen and L. L. Miller, *J. Am. Chem. Soc.*, 1989, **111**, 4105–4106.
20 V. Coropceanu, C. Lambert, G. Nöll and J.-L. Brédas, *Chem. Phys. Lett.*, 2003, **373**, 153–160.
21 S. F. Nelsen, R. F. Ismagilov, K. E. Gentile and D. R. Powell, *J. Am. Chem. Soc.*, 1999, **121**, 7108–7114.
22 S. F. Nelsen and H. Q. Tran, *J. Phys. Chem. A*, 1999, **103**, 8139–8144.
23 S. F. Nelsen, D. A. Trieber, R. F. Ismagilov and Y. Teki, *J. Am. Chem. Soc.*, 2001, **123**, 5684–5694.
24 S. F. Nelsen and R. F. Ismagilov, *J. Phys. Chem. A*, 1999, **103**, 5373–5378.
25 C. Creutz, M. D. Newton and N. Sutin, *J. Photochem. Photobiol., A*, 1994, **82**, 47–59.
26 C. Creutz, *Prog. Inorg. Chem.*, 1983, **30**, 1–73.
27 N. Sutin, *Prog. Inorg. Chem.*, 1983, **30**, 441–498.
28 B. S. Brunschwig and N. Sutin, in *Electron Transfer in Chemistry*, ed. V. Balzani, Wiley-VCH, Weinheim, 2001, vol. 2, pp. 583–617.
29 M. Renz, K. Theilacker, C. Lambert and M. Kaupp, *J. Am. Chem. Soc.*, 2009, **131**, 16292–16302.
30 M. D. Newton, *Adv. Chem. Phys.*, 1999, **106**, 303–375.
31 R. J. Cave and M. D. Newton, *J. Chem. Phys.*, 1997, **106**, 9213–9226.
32 R. J. Cave and M. D. Newton, *Chem. Phys. Lett.*, 1996, **249**, 15–19.
33 J. R. Reimers and N. S. Hush, *Chem. Phys.*, 1989, **134**, 323–354.
34 N. S. Hush, *Coord. Chem. Rev.*, 1985, **64**, 135–157.
35 N. S. Hush, in *Mixed-Valence Compounds*, ed. D. B. Brown, D. Reidel Publishing Company, Dordrecht, 1980, pp. 151–188.
36 B. S. Brunschwig, C. Creutz and N. Sutin, *Coord. Chem. Rev.*, 1998, **177**, 61–79.
37 B. J. Coe, J. A. Harris, B. S. Brunschwig, I. Asselberghs, K. Clays, J. Garin and J. Orduna, *J. Am. Chem. Soc.*, 2005, **127**, 13399–13410.
38 T. P. Treynor and S. G. Boxer, *J. Phys. Chem. A*, 2004, **108**, 1764–1778.
39 R. Wortmann, P. Krämer, C. Glania, S. Lebus and N. Detzer, *Chem. Phys.*, 1993, **173**, 99–108.
40 W. Liptay, in *Excited States*, ed. E. C. Lim, Academic Press, New York, 1974, vol. 1, pp. 129–229.
41 S. Beckmann, *et al.*, *Adv. Mater.*, 1999, **11**, 536–541.
42 P. Karafiloglou and J. P. Launay, *J. Phys. Chem. A*, 1998, **102**, 8004–8012.
43 W. Helal, S. Evangelisti, T. Leininger and D. Maynau, *J. Comput. Chem.*, 2009, **30**, 83–92.
44 N. Utz and T. Koslowski, *Chem. Phys.*, 2002, **282**, 389–397.
45 J. Seibt, A. Schaumlöffel, C. Lambert and V. Engel, *J. Phys. Chem. A*, 2008, **112**, 10178–10184.
46 D. R. Kattnig, B. Mladenova, G. Grampp, C. Kaiser, A. Heckmann and C. Lambert, *J. Phys. Chem. C*, 2009, **113**, 2983–2995.

47 S. Barlow, C. Risko, S.-J. Chung, N. M. Tucker, V. Coropceanu, S. C. Jones, Z. Levi, J.-L. Brédas and S. R. Marder, *J. Am. Chem. Soc.*, 2005, **127**, 16900–16911.
48 S. C. Jones, V. Coropceanu, S. Barlow, T. Kinnibrugh, T. Timofeeva, J.-L. Brédas and S. R. Marder, *J. Am. Chem. Soc.*, 2004, **126**, 11782–11783.
49 K. Lancaster, S. A. Odom, S. C. Jones, S. Thayumanavan, S. R. Marder, J.-L. Brédas, V. Coropceanu and S. Barlow, *J. Am. Chem. Soc.*, 2009, **131**, 1717–1723.
50 B. Strehmel, S. Amthor, J. Schelter and C. Lambert, *ChemPhysChem*, 2005, **6**, 893–896.
51 S. Amthor and C. Lambert, *J. Phys. Chem. A*, 2006, **110**, 3495–3504.
52 S. Amthor, C. Lambert, S. Dümmler, I. Fischer and J. Schelter, *J. Phys. Chem. A*, 2006, **110**, 5204–5214.
53 A. Heckmann, C. Lambert, M. Goebel and R. Wortmann, *Angew. Chem., Int. Ed.*, 2004, **43**, 5851–5856.
54 S. Barlow, *et al.*, *Chem. Commun.*, 2005, 764–766.
55 S. A. Odom, K. Lancaster, L. Beverina, K. M. Lefler, N. J. Thompson, V. Coropceanu, J.-L. Brédas, S. R. Marder and S. Barlow, *Chem.–Eur. J.*, 2007, **13**, 9637–9646.
56 S. J. Zheng, *et al.*, *J. Am. Chem. Soc.*, 2006, **128**, 1812–1817.
57 A. Heckmann and C. Lambert, *J. Am. Chem. Soc.*, 2007, **129**, 5515–5527.
58 D. Dehareng, G. Dive and A. Moradpour, *Int. J. Quantum Chem.*, 2000, **76**, 552–573.
59 E. Fernandez, L. Blancafort, M. Olivucci and M. A. Robb, *J. Am. Chem. Soc.*, 2000, **122**, 7528–7533.
60 S. Franzen and D. A. Shultz, *J. Phys. Chem. A*, 2003, **107**, 4292–4299.
61 S. F. Nelsen, M. N. Weaver, A. E. Konradsson, J. P. Telo and T. Clark, *J. Am. Chem. Soc.*, 2004, **126**, 15431–15438.
62 S. F. Nelsen and M. D. Newton, *J. Phys. Chem. A*, 2000, **104**, 10023–10031.
63 S. F. Nelsen and F. Blomgren, *J. Org. Chem.*, 2001, **66**, 6551–6559.
64 S. F. Nelsen, M. N. Weaver and J. P. Telo, *J. Am. Chem. Soc.*, 2007, **129**, 7036–7043.
65 A. Görling and M. Levy, *Phys. Rev. A: At., Mol., Opt. Phys.*, 1994, **50**, 196–204.
66 E. Engel and R. M. Dreizler, *J. Comput. Chem.*, 1999, **20**, 31–50.
67 R. J. Bartlett, I. Grabowski, S. Hirata and S. Ivanov, *J. Chem. Phys.*, 2005, **122**, 034104.
68 R. J. Bartlett, V. F. Lotrich and I. V. Schweigert, *J. Chem. Phys.*, 2005, **123**, 062205.
69 E. R. Johnson, P. Mori-Sanchez, A. J. Cohen and W. T. Yang, *J. Chem. Phys.*, 2008, **129**, 204112.
70 T. Heaton-Burgess and W. T. Yang, *J. Chem. Phys.*, 2010, **132**, 234113.
71 A. D. Becke, *J. Chem. Phys.*, 1993, **98**, 5648–5652.
72 See, *e.g.*: J. P. Perdew and K. Schmidt, in *Density Functional Theory and its Application to Materials*, ed. V. Van Doren, C. Van Alsenoy and P. Geerlings, AIP, Melville, New York, 2001; J. P. Perdew, A. Ruzsinszky, J. M. Tao, V. N. Staroverov, G. E. Scuseria and G. I. Csonka, *J. Chem. Phys.*, 2005, **123**, 062201; M. Kaupp, A. Arbuznikov and H. Bahmann, *Z. Phys. Chem.*, 2010, **224**, 545–567.
73 See, *e.g.*: T. M. Henderson, B. G. Janesko and G. E. Scuseria, *J. Phys. Chem. A*, 2008, **112**, 12530–12542, and references therein.
74 J. Jaramillo, G. E. Scuseria and M. Ernzerhof, *J. Chem. Phys.*, 2003, **118**, 1068–1073.
75 See, *e.g.*: H. Bahmann, A. Rodenberg, A. V. Arbuznikov and M. Kaupp, *J. Chem. Phys.*, 2007, **126**, 011103; A. V. Arbuznikov and M. Kaupp, *Chem. Phys. Lett.*, 2007, **440**, 160–168; A. V. Arbuznikov, H. Bahmann and M. Kaupp, *J. Phys. Chem. A*, 2009, **113**, 11898–11906; A. V. Arbuznikov, M. Kaupp and H. Bahmann, *J. Chem. Phys.*, 2006, **124**, 204102; A. Arbuznikov and M. Kaupp, *Int. J. Quantum Chem.*, 2011, **111**, 2625–2638; A. V. Arbuznikov and M. Kaupp, *J. Chem. Phys.*, 2008, **128**, 214107; M. Kaupp, A. Arbuznikov and H. Bahmann, *Z. Phys. Chem.*, 2010, **224**, 545–567.
76 A. D. Becke, *J. Chem. Phys.*, 2005, **122**, 064101.
77 A. D. Becke, *J. Chem. Phys.*, 2003, **119**, 2972–2977.
78 J. P. Perdew, V. N. Staroverov, J. Tao and G. E. Scuseria, *Phys. Rev. A: At., Mol., Opt. Phys.*, 2008, **78**, 052513.
79 A. V. Arbuznikov, H. Bahmann and M. Kaupp, *J. Phys. Chem. A*, 2009, **113**, 11898–11906.
80 R. M. Hoekstra, J. P. Telo, Q. Wu, R. M. Stephenson, S. F. Nelsen and J. I. Zink, *J. Am. Chem. Soc.*, 2010, **132**, 8825–8827.
81 J. P. Telo, S. F. Nelsen and Y. Zhao, *J. Phys. Chem. A*, 2009, **113**, 7730–7736.
82 S. F. Nelsen, K. P. Schultz and J. P. Telo, *J. Phys. Chem. A*, 2008, **112**, 12622–12628.
83 V. Barone and M. Cossi, *J. Phys. Chem. A*, 1998, **102**, 1995.
84 M. J. Frisch, *et al.*, *GAUSSIAN 03 (Revision E.01)*, Gaussian, Inc., Wallingford CT, 2004.
85 M. N. Mikhailov, A. S. Mendkovich, M. B. Kuminsky and A. I. Rusakov, *THEOCHEM*, 2007, **847**, 103–106.
86 S. F. Nelsen, M. N. Weaver, Y. Luo, J. V. Lockard and J. I. Zink, *Chem. Phys.*, 2006, **324**, 195–201.
87 S. F. Nelsen, Y. Luo, M. N. Weaver, J. V. Lockard and J. I. Zink, *J. Org. Chem.*, 2006, **71**, 4286–4295.
88 S. F. Nelsen, M. N. Weaver, J. I. Zink and J. P. Telo, *J. Am. Chem. Soc.*, 2005, **127**, 10611–10622.
89 S. F. Nelsen, A. E. Konradsson, M. N. Weaver and J. P. Telo, *J. Am. Chem. Soc.*, 2003, **125**, 12493–12501.
90 J. P. Telo, G. Grampp and M. Shohoji, *Phys. Chem. Chem. Phys.*, 1999, **1**, 99–104.
91 R. Ahlrichs, M. Bär, M. Häser, H. Horn and C. Köhmel, *Chem. Phys. Lett.*, 1989, **162**, 165–169.
92 A. D. Becke, *Phys. Rev. A: At., Mol., Opt. Phys.*, 1988, **38**, 3098–3100.
93 C. Lee, W. Yang and R. G. Parr, *Phys. Rev. B: Condens. Matter*, 1988, **37**, 785–789.
94 A. Schäfer, H. Horn and R. Ahlrichs, *J. Chem. Phys.*, 1992, **97**, 2571–2577.
95 A. Klamt and G. Schüürmann, *J. Chem. Soc., Perkin Trans. 2*, 1993, 799–805.
96 U. Varetto, *MOLEKEL 5.4*, Swiss National Supercomputing Centre, Manno (Switzerland).
97 E. Cancès and B. Mennucci, *J. Chem. Phys.*, 2001, **114**, 4744–4745.
98 M. J. Frisch, *et al.*, *GAUSSIAN 09 (Revision A.2)*, Gaussian, Inc., Wallingford CT, 2009.
99 W. Kutzelnigg, U. Fleischer and M. Schindler, in *NMR Basic Principles and Progress*, Springer-Verlag, Heidelberg, 1990, vol. 23, pp. 165–262.
100 V. G. Malkin, O. L. Malkina, R. Reviakine, A. V. Arbuznikov, M. Kaupp, B. Schimmelpfennig, I. Malkin, T. Helgaker and K. Ruud, *MAG-ReSpect, 2.1*, 2007.
101 A. Heckmann, S. Dümmler, J. Pauli, M. Margraf, J. Köhler, D. Stich, C. Lambert, I. Fischer and U. Resch-Genger, *J. Phys. Chem. C*, 2009, **113**, 20958–20966.
102 D. V. Matyushov and G. A. Voth, *J. Phys. Chem. A*, 2000, **104**, 6470–6484.
103 M. Ballester, I. Pascual and J. Torres, *J. Org. Chem.*, 1990, **55**, 3035–3044.

